STU
SLOVAK UNIVERSITY OF TECHNOLOGY IN BRATISLAVA

Journal of Electrical Engineering, Vol. 76, No. 5, 2025, pp. 398-408
https://reference-global.com/journal/JEE

Enhancing solar cell efficiency through contact replacement with advanced material

Ahmad Zhahirin Adly Bin Yaakob[1], Sim Sy Yi[1*], Kah Haw Law[2], Muhammad Aliff Hafeez Bin Azman[1], Alvin John Lim Meng Siang[3], Nur Sabrina Binti Azli Murzami[4]

This paper studies the impact of electrical contact placement and absorber materials on solar cell efficiency. Conventional front-contact designs cause shading losses, reducing light absorption. Using COMSOL Multiphysics, front-contact and back-contact solar cells were modelled with crystalline silicon and perovskite absorbers. Back-contact designs relocate all contacts to the rear, eliminating shading and improving absorption. Simulations under standard test conditions evaluated short-circuit current density, open-circuit voltage, output power density, and efficiency. Back-contact perovskite cells achieved the highest efficiency (20%), followed by back-contact crystalline silicon (13%) and front-contact crystalline silicon (10%). Results show that combining advanced materials with optimized contact layouts significantly enhances performance, providing valuable guidance for the design of efficient, scalable photovoltaic technologies.

Keywords: advanced material, COMSOL Multiphysics, contact placement, light absorption, solar cell

1 Introduction

Solar energy is one of the most promising renewable energy sources, playing a major role in reducing carbon emissions and reliance on fossil fuels. Currently, most of the world's energy still comes from fossil fuels like oil, natural gas, and coal, which release large amounts of CO_2 and contribute to global warming and climate change. Photovoltaic (PV) systems, which use solar panels to convert sunlight directly into electricity, are increasingly used in homes and businesses. As solar power demand rises, improving solar panel efficiency has become a key focus for researchers and manufacturers [1].

Since most appliances run on electricity, solar energy must be converted into electrical energy. This is done using solar cells, which operate based on the photovoltaic effect. When light hits a solar cell made from a p-n junction, photons with enough energy cause electrons to move, generating electricity [2, 3].

Solar energy has gained popularity due to advancements in technology, falling solar panel costs, and government incentives promoting renewables. Over recent decades, solar cell efficiency, which indicates how much sunlight is converted into electricity, has steadily increased [4]. However, PV systems still supply less than 0.03% of the world's total energy needs (~14 to 15 TW) [5]. To meet global energy demand, it is crucial to further improve solar cell efficiency, reduce production costs, and extend system lifespan. These efforts are vital to achieving "grid parity", where solar power becomes as cost-effective as electricity from the grid [5].

One major challenge in improving solar cell efficiency lies in the design of conventional front-contact solar cells, where electrical contacts (busbars) are placed on the front surface. While these metal strips collect and transport electricity, they also block part of the sunlight from reaching the active layer, leading to shading losses and reduced energy output [6]. Additionally, differences in thermal expansion between metals such as silver and silicon can cause stress at junction points, leading to microcracks, corrosion, and increased resistance over time, further lowering efficiency [7].

One innovative direction is the development of back contact solar cells, which are designed to capture more sunlight and reduce shading losses. Unlike conventional designs, back contact solar cells place both positive

[1] Faculty of Electrical and Electronic Engineering, Universiti Tun Hussein Onn Malaysia, 86400 Parit Raja, Batu Pahat Johor, Malaysia
[2] Electrical and Electronic Engineering Programme Area, Universiti Teknologi Brunei, Bandar Seri Begawan BE1410, Brunei
[3] Faculty of Civil Engineering and Built Environment, Universiti Tun Hussein Onn Malaysia, Johor, Malaysia
[4] Founder Energy Sdn Bhd, Klang, Selangor, Malaysia
sysim@uthm.edu.my

https://doi.org/10.2478/jee-2025-0042, Print (till 2015) ISSN 1335-3632, On-line ISSN 1339-309X

and negative electrodes on the rear side of the cell, eliminating front-side electrical contacts that block sunlight [8]. Enhancements to the back surface design also help reduce electrical resistance and improve performance [9]. Since R. J. Schwartz's initial research in 1975, interest in back contact cells has grown, and they are now gradually entering industrial applications [10].

In addition to better performance, back contact cells offer aesthetic advantages, making them ideal for applications where appearance matters. Without front-side electrical contacts or busbars, these panels have a sleek, modern look, which is ideal for integration into roofs, walls, and other visible surfaces. Technically, back contact designs also allow easier use of advanced materials and multi-junction structures like perovskite-silicon tandems. A cleaner front surface also allows better use of anti-reflective coatings and surface textures to improve light capture and reduce energy loss [10].

In this study, front-contact and back-contact solar cells were designed and simulated using COMSOL Multiphysics to evaluate the impact of contact placement and material choice on performance. Two absorber materials, which are crystalline silicon and perovskite, were tested. The objectives were to design and develop the proposed solar cell models, simulate and calculate the total energy output for each design, and evaluate and compare the efficiency of the proposed designs against conventional configurations.

It is important to note that the simulation is scaled down to simplify computation, which may limit direct comparison with full-scale devices. Material properties are assumed to be ideal and uniform, not accounting for real-world manufacturing defects or variations. Additionally, the models are two-dimensional, which cannot fully capture three-dimensional effects such as edge recombination, current crowding, or non-uniform illumination. Despite these constraints, the study provides valuable insights into how contact placement and material selection can influence solar cell performance.

2 Construction and working principle of solar cell

This section introduces the fundamental structure and operating principles of solar cells, which form the basis for the modeling and simulation tasks performed in this paper. It covers both conventional and advanced solar cell architectures, including front contact and back-contact designs. The section focuses on how sunlight interacts with the layers of the solar cell, how electricity is generated, and how it is separated and moved.

2.1 Conventional solar cell

A solar cell is primarily made from crystalline silicon, consisting of n-type and p-type semiconductor layers [11]. Typically, the top layer (emitter) is n-type silicon, and the bottom layer (base) is p-type, forming a p-n junction essential for electricity generation. To enhance light absorption, an anti-reflective coating is applied to reduce reflection losses. As shown in Fig. 1, this is the structure of a conventional front-contact solar cell, where the contacts are placed on the top surface to collect and conduct the generated current, while still allowing sunlight to pass through to the active layers.

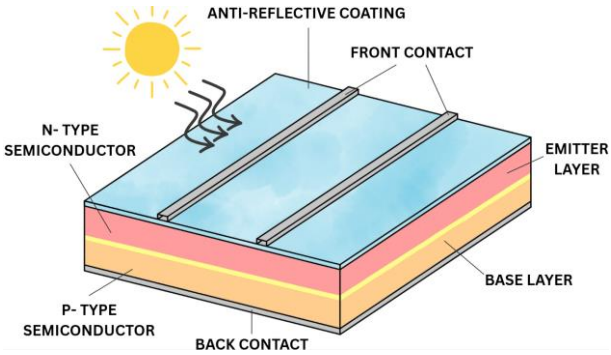

Fig. 1. Structure of a conventional solar cell

When sunlight strikes the cell, photons are absorbed by the semiconductor layers, generating electron-hole pairs. The electric field at the p-n junction drives electrons toward the n-type layer and holes toward the p-type layer. This charge separation produces electric current when the cell is connected to an external circuit [12].

Moreover, the n-type silicon is created by doping pure silicon with phosphorus, which donates free electrons to enhance conductivity. In contrast, p-type silicon is doped with boron, creating holes that act as positive charge carriers. As a result, when sunlight excites the electrons, they move through the circuit and generate electricity to power devices [5].

The solar cell structure in Fig. 2, which is used for simulation in this paper, includes multiple layers designed to enhance photovoltaic performance. Notably, it incorporates additional selective layers, an electron transport layer (ETL) and a buffer layer, which are to improve charge selectivity and reduce recombination losses.

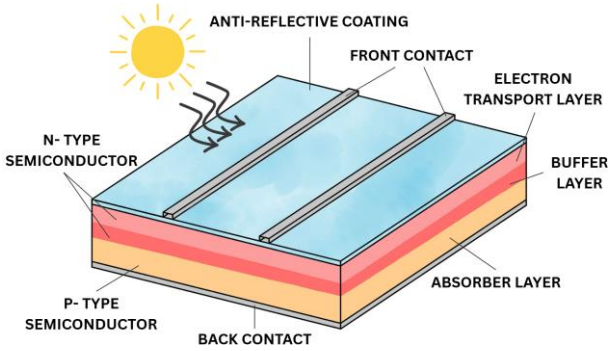

Fig. 2. Structure of a conventional solar cell with additional selective layers

Specifically, the ETL, located beneath the anti-reflective coating, guides electrons toward the front contact while blocking holes. This enhances charge separation and minimizes recombination, increasing efficiency. Furthermore, the buffer layer beneath the ETL improves the interface with the absorber by aligning energy levels and reducing defects that could trap charge carriers. Overall, these added layers help optimize carrier movement and reduce losses, which is expected to improve the cell's performance in the COMSOL simulation.

From Figs. 1 and 2, the differences between the conventional solar cell concept and the solar cell concept used in the simulation are clearly illustrated. In Fig. 1, the p-type and n-type semiconductors are silicon doped with boron and phosphorus, respectively. In contrast, the simulation concept as shown in Fig. 2 incorporates an additional buffer layer and electron transport layer, replacing the boron- and phosphorus-doped silicon. This approach aims to examine how the inclusion of two layers made from different materials can further enhance the efficiency of the solar cell.

2.2 Back-contact solar cell

The back-contact solar cell structure shown in Fig. 3, featuring an interdigitated back-contact design, is used for modelling in COMSOL. It captures sunlight through the top surface, which is coated with an anti-reflective layer to maximize light entry. Below this, the silicon absorber layer generates electron-hole pairs as sunlight excites electrons.

These charges are then separated by internal electric fields between the p-type and n-type regions within the absorber. Unlike conventional cells with front-side metal contacts that block some light, this design places all electrical contacts on the back in an interdigitated pattern, as illustrated in Fig. 3(b). As a result, both electrons and holes move toward the rear surface, where they are collected by their respective contacts, improving light absorption and overall efficiency.

As electrons move toward the n-type contact and the holes toward the p-type contact, the separation of these charge carriers generates an electric current. This current flows through an external circuit, delivering usable electrical power before the charges return to the cell and recombine [13].

The design benefits from having no shading on the front, excellent light absorption, and efficient charge collection due to reduced recombination, especially with the introduction of a rear passivation layer. This makes back-contact cells not only more efficient but also more visually appealing and effective in converting sunlight to electricity [13, 14].

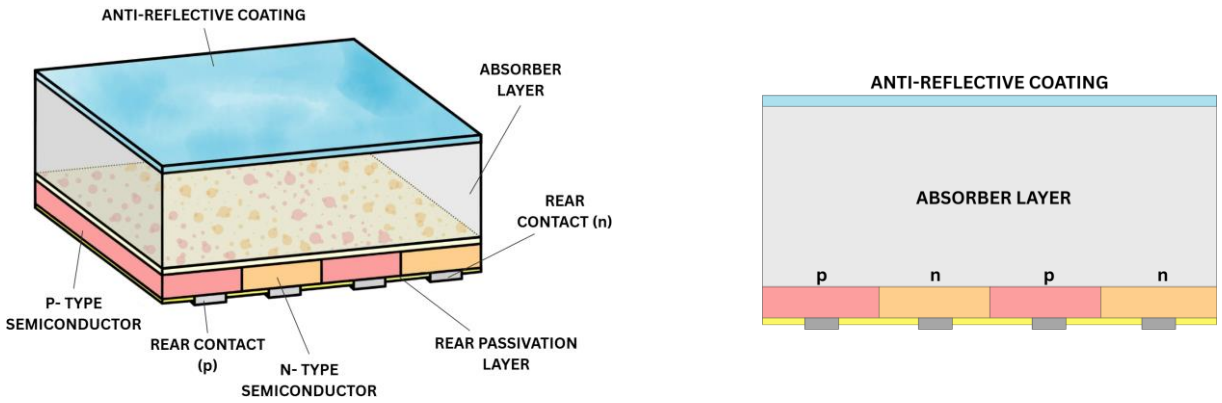

(a) (b)

Fig. 3. Structure of an interdigitated back-contact solar cell: (a) 3D view, (b) 2D view

2.3 Comparison between conventional front-contact and back-contact solar cells

The conventional front-contact solar cell and the interdigitated back-contact solar cell differ significantly in their design, shading losses, and charge collection efficiency, as shown in Tab. 1. The front-contact cell uses metal busbars and fingers on the front surface, which partially block incident light, leading to shading losses. In contrast, the back-contact cell relocates all electrical contacts to the rear, eliminating shading and improving light absorption. Additionally, the back-contact design allows for enhanced charge separation and collection due to its interdigitated contact layout, as well as the inclusion of advanced layers such as a rear passivation layer.

Table 1. Conventional front-contact vs. back-contact solar cells

Feature / Parameter	Conventional front-contact solar cell	Interdigitated back-contact solar cell
Contact placement	Front surface	Rear surface, interdigitated p- and n-contacts
Shading losses	Present due to front contact blockage	Eliminated, no front-side shading
Charge collection	Vertical collection toward front and rear	Lateral separation toward rear contacts

3 Methodology

The process of the project shown in Fig. 4. will consist of several phases of flow, which are designing, simulating, and comparing. These phases are very important because it helps decide how accurate and reliable the final simulation results will be. It is the key step that ensures the project works as planned and matches the real-world conditions.

This flowchart shows the step-by-step process of designing and testing front and back contact solar cells using COMSOL Multiphysics. The process starts with selecting where to place the electrical contacts, either on the front or back of the solar cell. Then, suitable materials are chosen, including their type (p-type or n-type) and doping levels, which affect how the solar cell works.

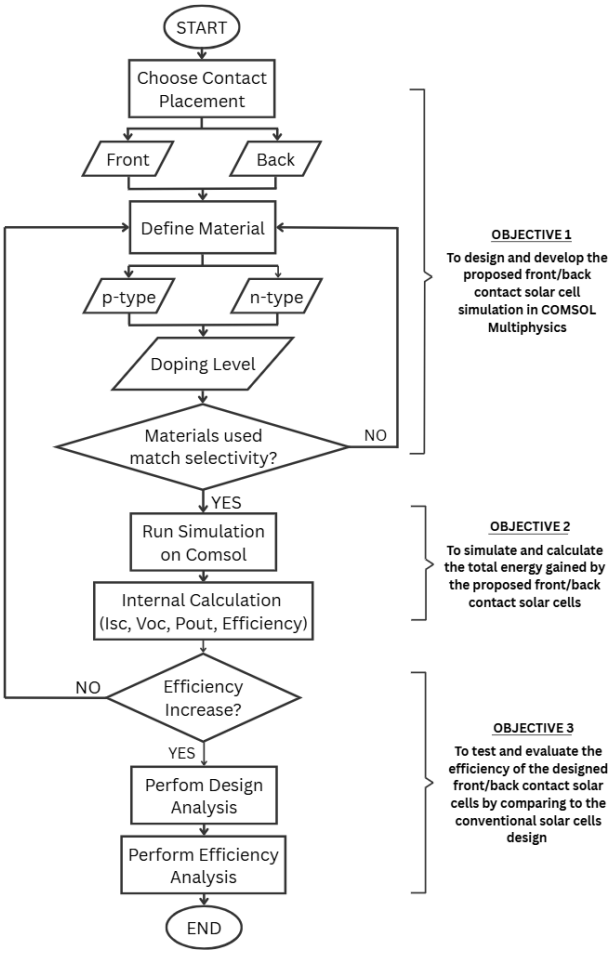

Fig. 4. Flowchart of project

Next, the materials are checked to make sure they are compatible, especially in terms of how well they align for energy flow and how effectively they separate electrical charges. If the materials are not suitable, the selection is adjusted. Once the materials are confirmed to be a good match, the solar cell is simulated using COMSOL.

The simulation produces key performance metrics such as short-circuit current (I_{SC}), open-circuit voltage (V_{OC}), power output (P_{OUT}), and efficiency. These results are evaluated to determine whether the new design performs better than the existing ones. If not, the process goes back to improving the design. If the design shows better efficiency, further analysis is done to understand why and how much it has improved.

This flowchart supports three main goals, which are to build the simulation model, to measure the performance of each design, and to compare the results with conventional solar cell designs to see if the new approach works better in enhancing efficiency, optimizing power output, and improving overall device performance.

3.1 Design setup

This section describes the fundamental configuration and modelling steps used to simulate the three solar cell models in COMSOL Multiphysics. This part focuses on establishing the geometric layout, assigning material properties, and defining the boundary and electrical conditions necessary to replicate the behavior of the solar cell under operational conditions.

3.1.1 Basic parameters and construction of front contact crystalline silicon

Figure 5 shows a front-contact crystalline silicon (c-Si) solar cell that uses a Zinc Oxide (ZnO) and Zinc Sulfide (ZnS) heterojunction structure. ZnO is placed at the top and works as the electron transport layer (ETL) because it conducts well and naturally behaves as an n-type material. Below it, ZnS acts as a buffer layer, helping to match energy bands and reduce unwanted charge recombination at the interface with the absorber layer.

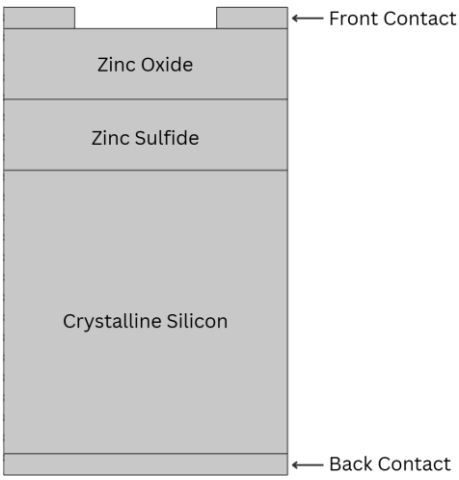

Fig. 5. Front-contact c-Si solar cell configuration

Table 2 presents the main electrical properties of the three key materials used in the front-contact crystalline silicon (c-Si) solar cell, which are ZnO, ZnS, and c-Si. The table lists essential semiconductor parameters, including relative permittivity, band gap, electron affinity, density of states for both the conduction and valence bands, as well as electron and hole mobilities and carrier lifetimes.

ZnO has a wide band gap of 3.3 eV, making it effective at transporting electrons while blocking holes, thus minimizing recombination at the front interface. ZnS, also characterized by a wide band gap, plays a critical role in improving energy band alignment between the ETL and the absorber. By smoothing the band offsets, ZnS reduces interface defects and minimizes carrier recombination, enhancing overall charge transfer efficiency. Crystalline silicon, with a smaller band gap of 1.15 eV and long carrier lifetimes, is the main layer that absorbs sunlight. These material parameters are incorporated into COMSOL Multiphysics to create an accurate simulation model, enabling precise evaluation of device behavior under different operating conditions and facilitating performance optimization of the solar cell design

3.1.2 Basic parameters and construction of back contact crystalline silicon

The geometry of the back-contact crystalline silicon solar cell was constructed in two dimensions to represent a simplified cross-section of the actual device, as shown in Fig. 6. The uppermost and largest rectangular section corresponds to the crystalline silicon absorber layer, which is responsible for capturing incident sunlight and generating electron–hole pairs through the photovoltaic effect. Its thickness and material properties are defined to maximize photon absorption while minimizing recombination losses.

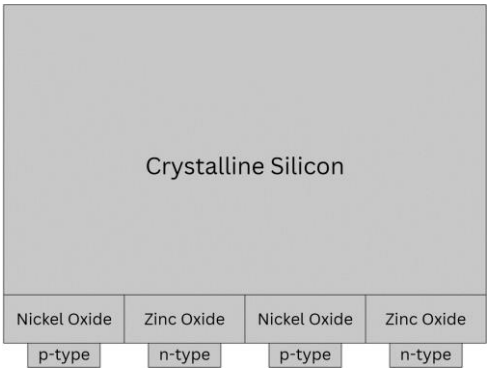

Fig. 6. Back-Contact c-Si Solar Cell Configuration

Directly beneath the absorber, alternating vertical segments of Nickel Oxide (NiO_x) and ZnO are arranged to form the hole transport layer (HTL) and electron transport layer (ETL), respectively. This repeating p-n-p-n configuration establishes the interdigitated back-contact (IBC) architecture, where each material selectively extracts one type of charge carrier

Completing the structure, smaller rectangular metallic contact blocks are placed directly below each NiO_x and ZnO region. These serve as the electrical terminals for the p-type and n-type regions, providing well-defined, low-resistance pathways for the extracted charges to flow into an external circuit during simulation. The rear-only contact configuration eliminates the need for front-side metallization, thereby avoiding shading losses and allowing the entire front surface to be dedicated to light absorption. This combination of full-surface illumination and efficient carrier separation is expected to improve overall device efficiency compared to conventional front-contact designs.

Table 2. Material parameters for ZnO, ZnS, and c-Si in front-contact solar cell design

	ZnO	ZnS	c-Si
Relative permittivity	9	8.9	13.6
Band gap (eV)	3.3	3.7	1.15
Electron affinity (eV)	4.3	3.9	4.5
Effective density of states, valence band ($1/cm^3$)	2.9×10^{19}	1×10^{19}	1×10^{19}
Effective density of states, conduction band ($1/cm^3$)	2.9×10^{19}	2×10^{18}	1×10^{19}
Electron mobility (cm^2/Vs)	200	100	100
Hole mobility (cm^2/Vs)	5	10	25
Electron lifetime (ns)	10	5	5
Hole lifetime (ns)	10	5	5

Table 3 presents the key electrical and material properties of ZnO, NiO_x, and c-Si used in the inter-digitated back-contact solar cell. ZnO serves as the electron transport layer (ETL) due to its high electron mobility, wide band gap of 3.3 (eV), and excellent optical transparency, enabling efficient electron extraction while blocking holes to reduce recombination losses. NiO_x, with its wide band gap and high hole mobility, replaces ZnS as the hole transport layer (HTL) to provide better energy band alignment with c-Si and enhanced compatibility with the back-contact structure, thereby facilitating efficient hole extraction. Crystalline silicon remains the main absorber for its excellent carrier lifetime and proven efficiency. Together, ZnO and NiO_x enable effective carrier separation and selective charge collection at the back contacts.

3.1.3 Basic parameters and construction of back contact perovskite

The back-contact perovskite solar cell, shown in Fig. 7, adopts an interdigitated architecture similar to the crystalline silicon design, where alternating p-type and n-type transport layers are positioned at the rear of the absorber. Constructed in a 2D geometry, the model includes a large top block representing the perovskite absorber layer, specifically methylammonium lead iodide ($MAPbI_3$), known for its high absorption coefficient and tunable band gap. Below this absorber layer, alternating narrow blocks of Spiro-OMeTAD (p-type) and titanium dioxide (TiO_2, n-type) are arranged in a repeating p-n-p-n pattern.

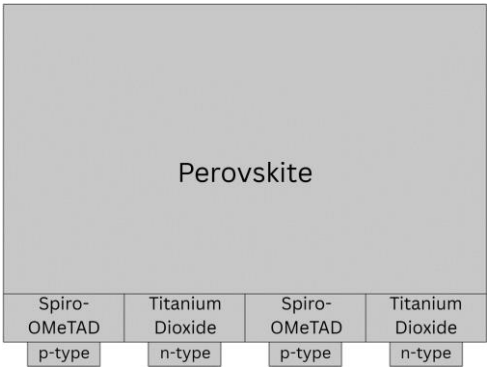

Fig. 7. Back-contact perovskite solar cell configuration

These transport layers play a critical role in selectively extracting holes and electrons while minimizing recombination losses. TiO_2 has a wide band gap and high permittivity, making it suitable for electron transport and hole blocking. Spiro-OMeTAD, with a lower electron affinity and moderate band gap, serves as an effective hole transporter. Small rectangular contact regions are placed directly below the transport layers. These act as electrical terminals to enable current flow through the device under simulation, providing low-resistance pathways for charge carriers to exit the solar cell.

Table 3. Material parameters for ZnO, NiO_x, and c-Si in front-contact solar cell design

	ZnO	NiO_x	c-Si
Relative permittivity	9	11.9	13.6
Band gap (eV)	3.3	3.6	1.15
Electron affinity (eV)	4.3	1.46	4.5
Effective density of states, valence band ($1/cm^3$)	2.9×10^{19}	2.5×10^{19}	1×10^{19}
Effective density of states, conduction band ($1/cm^3$)	2.9×10^{19}	2.5×10^{19}	1×10^{19}
Electron mobility (cm^2/Vs)	200	1	100
Hole mobility (cm^2/Vs)	5	2.5	25
Electron lifetime (ns)	10	5	5
Hole lifetime (ns)	10	10	5

The layout also ensures that all extracted carriers are directed to their respective terminals efficiently, resulting in higher simulated power output and device performance.

Table 4 outlines the key material properties of the three materials used in the perovskite solar cell, which are Spiro-OMeTAD (HTL), perovskite (absorber), and TiO_2 (ETL). Parameters include relative permittivity, band gap, electron affinity, density of states, carrier mobilities, and lifetimes are essential for accurate COMSOL simulation. The perovskite layer, with a 1.52 eV band gap and high dielectric constant, ensures strong light absorption and efficient carrier separation. TiO_2, with a wide band gap and high permittivity, effectively transports electrons and blocks holes. Lastly, Spiro-OMeTAD, with a lower electron affinity and 3 eV band gap, serves as the hole transport material. Together, these materials enable efficient charge generation, separation, and collection.

3.2 Fundamental equations for photovoltaic analysis

In a solar cell, the open-circuit voltage V_{OC} is derived from the balance between the photocurrent I_{SC} generated by absorbed photons and the dark saturation current I_S, which is a result of thermal recombination. Under open-circuit conditions, the net current through the solar cell is zero because no external circuit allows current flow [15]. The voltage is determined by the diode equation under open-circuit conditions based on Eqn. 1.

$$V_{OC} = \frac{kT}{q} \ln\left(\frac{I_{SC}}{I_S} + 1\right) \quad (1)$$

Here, k is the Boltzmann constant, T is temperature in Kelvin, q is the electron charge, I_{SC} represents the short-circuit current, and I_S represents the saturation current.

Next, the short-circuit current I_{SC} is produced by the collection of light-generated carriers in a solar cell. In an ideal cell with minimal resistive losses, I_{SC} equals the light-generated current, representing the maximum current output.

For cells made from the same material, I_{SC} mainly depends on carrier diffusion lengths and surface passivation quality. With perfect passivation and uniform generation, the short-circuit current density J_{SC} can be estimated using Eqn. 2.

$$J_{SC} = \frac{I_{SC}}{A}, \quad (2)$$

where I_{SC} is the short circuit current, and A is the illuminated area.

Furthermore, the input power of a solar cell refers to the amount of sunlight (solar radiation) it receives, typically measured in watts per unit area. This value is determined by several factors, including solar irradiance and surface area of the solar cell [16]. Thus, it is calculated as the formula shown in Eqn. 3

$$P_N = E \cdot A, \quad (3)$$

where E is the solar irradiance, typically 1000 W/m^2 under standard test conditions, and A is the active area of the solar cell, in m^2.

Table 4. Material parameters for Spiro-OMETAD, TiO_2, and perovskite in back-contact solar cell design

	Spiro-OMeTAD	Perovskite	TiO_2
Relative permittivity	3	18	31
Band gap (eV)	3	1.52	3
Electron affinity (eV)	1.9	3.6	4.1
Effective density of states, valence band (1/cm^3)	1×10^{20}	5×10^{18}	1×10^{20}
Effective density of states, conduction band (1/cm^3)	1×10^{20}	5×10^{18}	1×10^{20}
Electron mobility (cm^2/Vs)	2	2	1×10^{-2}
Hole mobility (cm^2/Vs)	1×10^{-2}	2	2
Electron lifetime (ns)	5	100	5
Hole lifetime (ns)	5	100	5

The output power is the actual electrical power generated by the solar cell at its maximum power point, where the product of voltage and current is maximized [17]. The relationship between the voltage and current is described by the Eqn. 4.

$$P_{OUT} = V_{OC} \cdot \frac{I_{SC}}{A} \quad (4)$$

in which V_{OC} represents the open-circuit voltage, and I_{SC} divided by illuminated area, A is the short-circuit current density.

Lastly, efficiency is the final parameter simulated in this study, as it reflects the overall performance of the solar cell in converting sunlight into usable electrical energy. Solar cell efficiency refers to the ability of the solar cell to convert sunlight into usable electrical energy. It is a measure of how effectively the solar cell captures and utilizes the energy from sunlight to generate power [17], and it can be found with the formula from Eqn. 5.

$$\eta = \frac{P_{OUT}}{P_{IN}} \cdot 100 \quad (5)$$

Consequently, the process of the project is important as it ensures a systematic approach to designing and simulating solar cells, enabling accurate performance analysis. Besides, the formula used to calculate key parameters are essential for evaluating the impact of design changes and validating the effectiveness of different contact placements. These calculations help evaluate the designs and compare the results to understand how different contact placements affect the solar cell's performance.

4 Results and discussion

This section presents the results from 2D solar cell simulations using COMSOL Multiphysics. Key performance parameters such as open-circuit voltage (V_{OC}), short-circuit current density (J_{SC}), and power output density were calculated. Finally, the efficiency of each model was compared to evaluate the performance of the three solar cell designs.

4.1 Short-circuit current density curve

The comparative *J-V* curve in Fig. 8 illustrates the terminal current behavior of three different solar cell configurations, which are front-contact c-Si, back-contact c-Si, and back-contact perovskite, across a range of applied voltages. This graph highlights the influence of both material selection and contact architecture on the photocurrent generation performance. Figure 8 also shows the terminal current vs. applied voltage for front-contact and back-contact solar cell models using different materials.

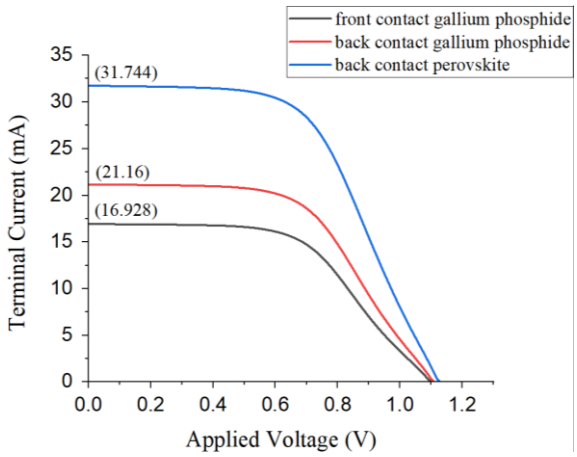

Fig. 8. Comparison of J_{SC} curve for front-contact and back-contact solar cell designs using different materials

At zero voltage (short-circuit condition), the back-contact perovskite cell shows the highest current at approximately 32 mA, followed by back-contact c-Si at 21 mA, and front-contact c-Si at 17 mA. The perovskite model performs best due to its strong light absorption and efficient charge generation. Both back-contact designs benefit from the absence of front-side shading, allowing more light capture than the front-contact design.

Furthermore, all three models show a typical drop in current as voltage approaches open-circuit conditions. The recorded V_{OC} values are 1.1 V for front-contact c-Si, 1.11 V for back-contact c-Si, and 1.12 V for back-contact perovskite, with similar voltage characteristics but differing current outputs.

This comparison highlights the significant impact of contact placement and absorber material on current generation. The back-contact perovskite model achieves the best performance, while the front-contact c-Si model is limited by shading and higher recombination losses.

4.2 Power output density curve

The power-voltage graph in Fig. 9 compares three solar cell configurations, which are front-contact c-Si, back-contact c-Si, and back-contact perovskite. It illustrates how both material choice and contact design influence power output. The back-contact perovskite cell achieves the highest power at its maximum power point (MPP), producing 199 W/m² at 0.72 V. This is followed by the back-contact c-Si at 130 W/m² and the front-contact c-Si at 103 W/m², both at 0.7 V.

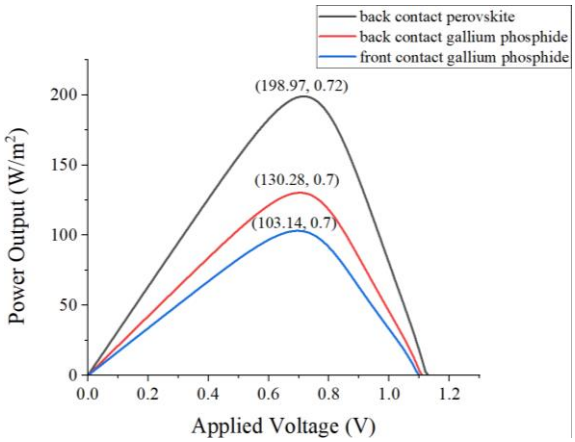

Fig. 9. Comparison of P-V Curve for front-contact and back-contact solar cell designs using different materials

The superior performance of the perovskite model is due to its strong light absorption and low recombination losses. The back-contact design used in both perovskite and c-Si models eliminates front-side shading, enhancing light capture. In contrast, the front-contact c-Si model suffers power loss due to shading from metal contacts. All three curves show the expected P–V shape, peaking at the maximum power point (MPP) and dropping toward zero near the open-circuit voltage, indicating stable photovoltaic behavior.

Overall, the graph confirms the advantage of the back-contact perovskite design for achieving higher power output and its strong potential for high-efficiency solar applications.

4.3 Efficiency curve

The efficiency-voltage graph in Fig. 10 illustrates the energy conversion performance of three solar cell configurations, which are front-contact c-Si, back-contact c-Si, and back-contact perovskite. Each curve displays the characteristic parabolic shape, reaching its peak at the model's respective maximum power point (MPP). Figure 10 also presents a comparison of efficiency percentages for these solar cell designs using

different materials and contact configurations, highlighting how variations in absorber type, transport layers, and electrode placement influence overall energy conversion capability.

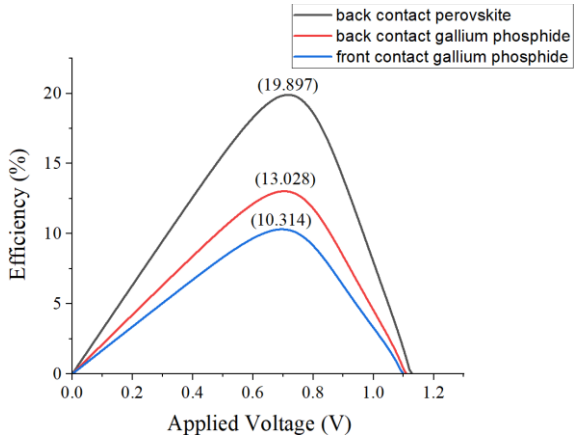

Fig. 10. Comparison of efficiency for front-contact and back-contact solar cell designs using different materials

Among the three designs, the back-contact perovskite solar cell achieves the highest efficiency at almost 20%, followed by the back-contact c-Si at 13%, and the front-contact c-Si at 10%. The superior performance of the perovskite model is due to its strong light absorption across a broad spectrum, low recombination losses due to longer carrier lifetime, and contact placement that avoids front-side shading, allowing more sunlight to reach the absorber layer.

The back-contact c-Si also outperforms the front-contact version, which suffers efficiency loss from shading by front metal contacts. These results confirm that both material selection and contact placement significantly affect efficiency. The back-contact perovskite design stands out as the most efficient, showing strong potential for next-generation photovoltaic technologies.

Furthermore, the results of the parameters simulated for each solar cell model are tabled in Tab. 5, showing the short-circuit current (I_{SC}), open-circuit voltage (V_{OC}), output power (P_{OUT}), and efficiency for front-contact crystalline silicon, back-contact crystalline silicon, and back-contact perovskite designs. Table 5 summarizes the results obtained from the three models of solar cell simulation, providing a direct comparison of their key performance metrics and enabling a clear assessment of how each design variation influences overall efficiency and power generation capability.

Table 5. Summary of simulated parameters for the designed solar cell model

	I_{SC} (mA)	V_{OC} (V)	P_{OUT} (W/m^2)	Efficiency (%)
Front-contact c-Si	17	1.1	103	10
Back-contact c-Si	21	1.11	130	13
Back-contact perovskite	32	1.12	199	20

5 Conclusion

This study explored the influence of contact placement and material selection on solar cell performance through COMSOL Multiphysics simulations. Three configurations were examined: a conventional front-contact crystalline silicon cell, a back-contact crystalline silicon cell, and a back-contact perovskite cell. The simulation results revealed that relocating the electrical contacts to the rear of the cell significantly improves performance by eliminating front-side shading and enhancing charge collection. Notably, the back-contact perovskite cell achieved the highest efficiency of approximately 20%, outperforming both the back-contact crystalline silicon (13%) and the front-contact crystalline silicon design (10%).

The key scientific contribution of this work lies in demonstrating how the integration of an interdigitated back-contact layout and advanced materials such as perovskite, TiO_2, and Spiro-OMeTAD can synergistically enhance photovoltaic efficiency. Compared to conventional designs, the proposed configurations offer improved current density, power output, and optical absorption. These findings are consistent with existing literature and reinforce the importance of contact engineering in solar cell design.

This work contributes to the ongoing development of high-efficiency, scalable solar technologies and provides valuable insights for future research on optimizing material combinations and geometries for next-generation photovoltaic devices.

Acknowledgement

This research is supported by Ministry of Higher Education (MOHE) through Fundamental Research Grant Scheme (FRGS/1/2024/TK08/UTHM/03/9).

References

[1] G. K. Dalapati, S. Ghosh, T. S. P. A, B. Ramasubramanian, A. Samanta, A. Rathour, T. K. S. Wong, S. Chakrabortty, S. Ramakrishna, and A. Kumar, "Maximizing solar energy production in ASEAN region: Opportunity and challenges," Results in Engineering, vol. 20, p. 101525, Dec. 2023, doi: 10.1016/j.rineng.2023.101525.

[2] M. M. Hasan, S. Hossain, M. Mofijur, Z. Kabir, I. A. Badruddin, T. M. Y. Khan, and E. Jassim, "Harnessing solar power: A review of photovoltaic innovations, solar thermal systems, and the dawn of energy storage solutions," Energies, vol. 16, no. 18, p. 6456, Sep. 2023, doi: 10.3390/en16186456.

[3] F. Fadliondi, B. Budiyanto, and P. G. Chamdareno, "The improvement of solar panel performance using cooling method," Trends in Sciences, vol. 20, no. 11, Aug. 2023, doi: 10.48048/tis.2023.6710.

[4] F. A. Ansari, A. Haleem, S. Bahl, M. Javaid, D. Buddhi, C. Prakash, and R. C. Sharma, "Advancement in solar energy technology and its future growth," in Advances in Fluid and Thermal Engineering: Select Proceedings of FLAME 2022, B. S. Sikarwar, S. K. Sharma, A. Jain, and K. M. Singh, Eds. Singapore: Springer, 2023, pp. 347–357, doi: 10.1007/978-981-99-2382-3_29.

[5] D. S. Ginley, R. Collins, and D. Cahen, "Direct solar energy conversion with photovoltaic devices," in Fundamentals of Materials for Energy and Environmental Sustainability, D. S. Ginley and D. Cahen, Eds. Cambridge: Cambridge University Press, 2011, pp. 216–237

[6] N. Amin, S. Santhiran, N. M. Kassim, A. A. Alkahtani, M. A. Islam, and M. Y. M. Yusof, "Impact analysis of metallization design and recombination losses on performance of crystalline silicon solar cells," Energies, vol. 16, no. 18, p. 6505, Sep. 2023, doi: 10.3390/en16186505.

[7] L. C. Rendler, A. Kraft, C. Ebert, U. Eitner and S. Wiese, "Mechanical stress in solar cells with multi busbar interconnection – Parameter study by FEM simulation," 2016 17th International Conference on Thermal, Mechanical and Multi-Physics Simulation and Experiments in Microelectronics and Microsystems (EuroSimE), Montpellier, France, 2016, pp. 1-5, doi: 10.1109/EuroSimE.2016.7463325.

[8] W. Ahmad, C. Li, W. Yu, and P. Gao, "Revolutionizing photovoltaics: From back-contact silicon to back-contact perovskite solar cells," Materials Today Electronics, vol. 9, p. 100106, Sep. 2024, doi: 10.1016/j.mtelec.2024.100106.

[9] P. Tang, Z.-H. Huang, L.-J. Liu, L.-M. Lin, Q.-Y. Ye, D. Wei, S.-Y. Chen, and G.-L. Chen, "Modifying back contact by silver to enhance the performance of carbon-based Sb_2S_3 solar cells," Appl. Surf. Sci., vol. 677, Art. No. 160960, Dec. 2024, doi: 10.1016/j.apsusc.2024.160960.

[10] E. Van Kerschaver and G. Beaucarne, "Back-contact solar cells: A review," Progress in Photovoltaics: Research and Applications, vol. 14, no. 2, pp. 107–123, Mar. 2006, doi: 10.1002/pip.657.

[11] M. A. Hanif, F. Nadeem, R. Tariq, and U. Rashid, "Chapter 4 - Solar thermal energy and photovoltaic systems," in Renewable and Alternative Energy Resources, Academic Press, 2022, pp. 171–261. doi: 10.1016/B978-0-12-818150-8.00007-1.

[12] N. Guerra, M. Guevara, C. P. Arias, and F. Crupi, "Operation and physics of photovoltaic solar cells: an overview," I+D Tecnológico, vol. 14, no. 2, pp. 84–95, Dec. 2018, doi: 10.33412/idt.v14.2.2077.

[13] [13] M. K. Mat Desa et al., "Silicon back contact solar cell configuration: A pathway towards higher efficiency," Renewable and Sustainable Energy Reviews, vol. 60, pp. 1516–1532, Jul. 2016, doi: 10.1016/j.rser.2016.03.004.

[14] W. Ahmad, C. Li, W. Yu, and P. Gao, "Revolutionizing photovoltaics: From back-contact silicon to back-contact perovskite solar cells," Materials Today Electronics, vol. 9, 100106, Sep. 2024, doi: 10.1016/j.mtelec.2024.100106.

[15] P. Baruch, A. De Vos, P. T. Landsberg, and J. E. Parrott, "On some thermodynamic aspects of photovoltaic solar energy conversion," Solar Energy Materials and Solar Cells, vol. 36, no. 2, pp. 201–222, Feb. 1995, doi: 10.1016/0927-0248(95)80004-2.

[16] A. Cuevas, "The Recombination Parameter J_0," *Energy Procedia*, vol. 55, pp. 53–62, 2014, doi: 10.1016/j.egypro.2014.08.073.

[17] S. Sugianto, "Comparative analysis of solar cell efficiency between monocrystalline and polycrystalline," INTEK J. Penelit., vol. 7, no. 2, p. 92, Dec. 2020, doi: 10.31963/intek.v7i2.2625.

Received 29 June 2025